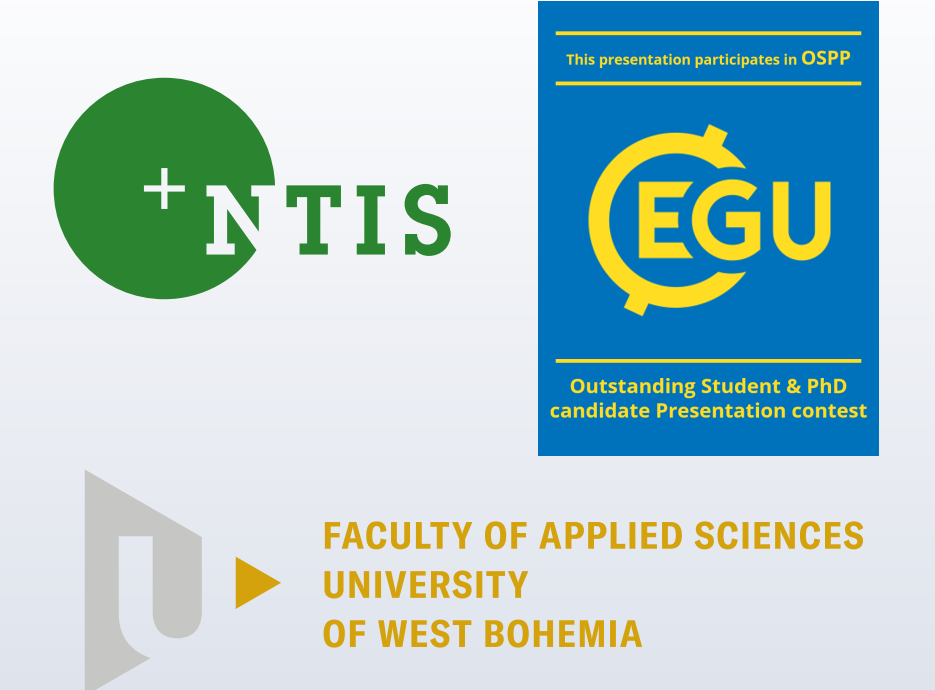


Global gravitational field modelling for spheroidal planetary bodies: non-singular solutions

Jiří Belinger, Veronika Dohnalová, Martin Pitoňák, Pavel Novák, Michal Šprlák

NTIS – New Technologies for the Information Society, Faculty of Applied Sciences, University of West Bohemia in Pilsen, Technická 8, 306 14 Plzeň, Czech Republic, belinger@ntis.zcu.cz



Introduction

Determination of gravitational fields generated by various planetary bodies (including Earth, Earth's Moon or neighboring planets) represents a crucial task in modern geodesy and planetology. In most cases, calculation of gravitational field quantities is based on the spherical approximation of planetary bodies. Spherical approximation is valid for bodies with shapes close to sphere or in cases when lower gravitational field quantities estimation accuracy is acceptable.

On the other hand, shapes of planetary bodies are often closer to spheroids. The spheroidal approximation is essential as it significantly extends region near the surface of flattened planetary bodies (Fig. 1) allowing safe computation without any divergence issues.

This contribution describes theoretical and numerical aspects for the gravitational field modelling of planetary bodies using spheroidal harmonic synthesis. We focus on the substitution of singular expressions (containing partial derivatives with respect to reduced spheroidal latitude β and trigonometric functions dependent on β) occurring in calculations by non-singular recursive expressions. We consider both oblate and prolate spheroids. However, for brevity, we focus exclusively on oblate geometry in this poster.

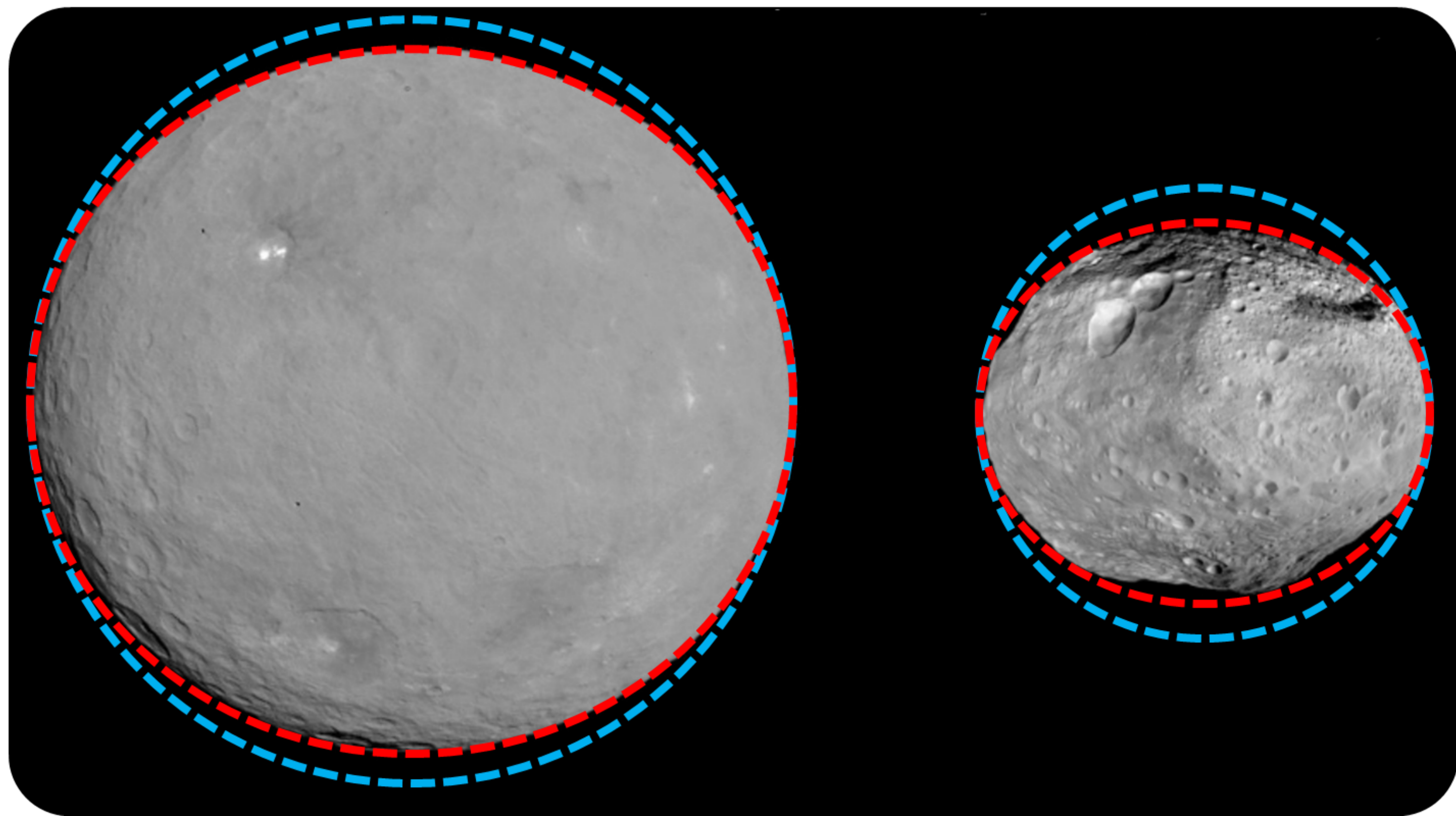


Fig. 1: Difference between spherical (blue) and spheroidal (red) approximation for the dwarf planet Ceres (left) and asteroid Vesta (right).

Theoretical background

Principles of deriving the relevant formulas can be described using Eq. (1) that represents the first-order partial derivative of gravitational potential V with respect to β (V_β), as it is the most concise equation allowing to explain all important parts of the above-mentioned process solving singularities. The specific form of the equation is as follows:

$$V_\beta(u, \Omega) = \frac{GM}{R_o} \sum_{n=0}^{\infty} \sum_{m=-n}^n \bar{C}_{n,m}^o(u) \frac{Q_{n,|m|}(\frac{i^u}{\varepsilon})}{Q_{n,|m|}(\frac{i^b}{\varepsilon})} \frac{1}{L} \frac{\partial}{\partial \beta} \bar{P}_{n,|m|}(\sin \beta) K_m(\lambda) + \frac{GM}{R_i} \sum_{n=0}^{\infty} \sum_{m=-n}^n \bar{C}_{n,m}^i(u) \frac{P_{n,|m|}(\frac{i^u}{\varepsilon})}{P_{n,|m|}(\frac{i^b}{\varepsilon})} \frac{1}{L} \frac{\partial}{\partial \beta} \bar{P}_{n,|m|}(\sin \beta) K_m(\lambda), \quad (1)$$

where (u, Ω) are the Jacobi one-parametric coordinates of a computational point. GM is the geocentric gravitational constant. R_o and R_i are suitable scale factors, n and m stand for degree and order of the spheroidal harmonic expansion. $\bar{C}_{n,m}^o$ and $\bar{C}_{n,m}^i$ denote the normalized (geodetic norm) spheroidal harmonic coefficients. $P_{n,|m|}$ and $Q_{n,|m|}$ define the un-normalized ($\bar{P}_{n,|m|}$ for normalized, respectively) associated Legendre functions of the first and the second kind. ε stands for the linear eccentricity calculated from major and minor semi-axes of the reference spheroid a and b , $L = \sqrt{u^2 + \varepsilon^2 \sin^2 \beta}$ and:

$$K_m(\lambda) = \begin{cases} \cos m\lambda, & m \geq 0, \\ \sin |m|\lambda, & m < 0. \end{cases} \quad (2)$$

Equation (1) consists of 2 main parts:

- Calculation outside the confocal spheroid with minor semi-axis u (upper part),
- Calculation inside the confocal spheroid with minor semi-axis u , but outside gravitating masses (lower part).

In case of Eq. (1), it was necessary to apply specific recursions substituting $\frac{\partial}{\partial \beta} \bar{P}_{n,|m|}(\sin \beta)$. The final form of Eq. (1) after the implementation of these recursions is:

$$V_\beta(u, \Omega) = \frac{GM}{2R_o L} \sum_{n=1}^{\infty} \bar{C}_{n,0}^o(u) \frac{Q_{n,0}(\frac{i^u}{\varepsilon})}{Q_{n,0}(\frac{i^b}{\varepsilon})} \sqrt{2n(n+1)} \bar{P}_{n,1}(\sin \beta) + \frac{GM}{2R_o L} \sum_{n=1}^{\infty} \sum_{\substack{m=-n \\ m \neq 0}}^n \bar{C}_{n,m}^o(u) \frac{Q_{n,|m|}(\frac{i^u}{\varepsilon})}{Q_{n,|m|}(\frac{i^b}{\varepsilon})} \left[\sqrt{(n-|m|)(n+|m|+1)} \bar{P}_{n,|m|+1}(\sin \beta) - \sqrt{(1+\delta_{|m|,0})(n+|m|)(n-|m|+1)} \bar{P}_{n,|m|-1}(\sin \beta) \right] K_m(\lambda) + \dots, \quad (3)$$

where $\delta_{n,m}$ is the Kronecker delta. Only the outer part of Eq. (3) is presented, as implementation of recursions for the inner part is analogical and can be deduced from Eqs. (1) and (3).

Equivalent equations (singular and non-singular) were derived for all other derivatives of the gravitational potential up to the third order (3 for the gravitational gradient vector, 6 for the second-order gravitational tensor and 10 for the third-order gravitational tensor).

Numerical experiment

Equations described in previous section, together with all analogical equations concerning other derivatives of the gravitational potential were implemented into C language scripts. Using these scripts, it was possible to carry out an experiment testing correctness of both theory and its implementation. The basic assumption was that comparison between singular and non-singular expressions should indicate very low differences with exception of polar regions, where the singular solution accuracy was expected to decrease rapidly. To compare results over non-polar region ($-80^\circ \leq \beta \leq 80^\circ$), testing grids were synthesized from EGM2008 to the maximal degree $n = 360$ over the 0.1° equiangular grid. The differences were studied for 10 third-order derivatives of the gravitational potential. Resulting statistics are available in Tab. 1. All signal values concerning comparison were in $10^{-15} m^{-1} s^{-2}$.

Tab. 1: Statistics of the differences over non-polar region. All values are given in $10^{-27} m^{-1} s^{-2}$.

Derivative	mean	std	min	max	Derivative	mean	std	min	max
V_{uuu}	0.01	8.87	-111.40	94.96	$V_{u\lambda\lambda}$	0.00	3.04	-35.00	36.08
$V_{uu\beta}$	-0.03	7.99	-85.15	100.10	$V_{\beta\beta\beta}$	-0.02	7.20	-93.04	70.00
$V_{uu\lambda}$	0.00	3.86	-42.75	45.13	$V_{\beta\beta\lambda}$	0.00	1.91	-25.95	20.25
$V_{u\beta\beta}$	-0.02	7.54	-95.10	111.53	$V_{\beta\lambda\lambda}$	0.00	1.44	-19.06	17.14
$V_{u\beta\lambda}$	0.00	2.38	-36.46	31.51	$V_{\lambda\lambda\lambda}$	0.00	2.79	-66.40	68.83

In the next step, the rapid increase of differences in regions close to the poles showing inaccuracies in singular solution had to be proven. Some of the derivatives without dependencies on β indicated no singularities. However, with the increase in dependence there was also significant increase in order of magnitude of corresponding differences as demonstrated in Fig. 2.

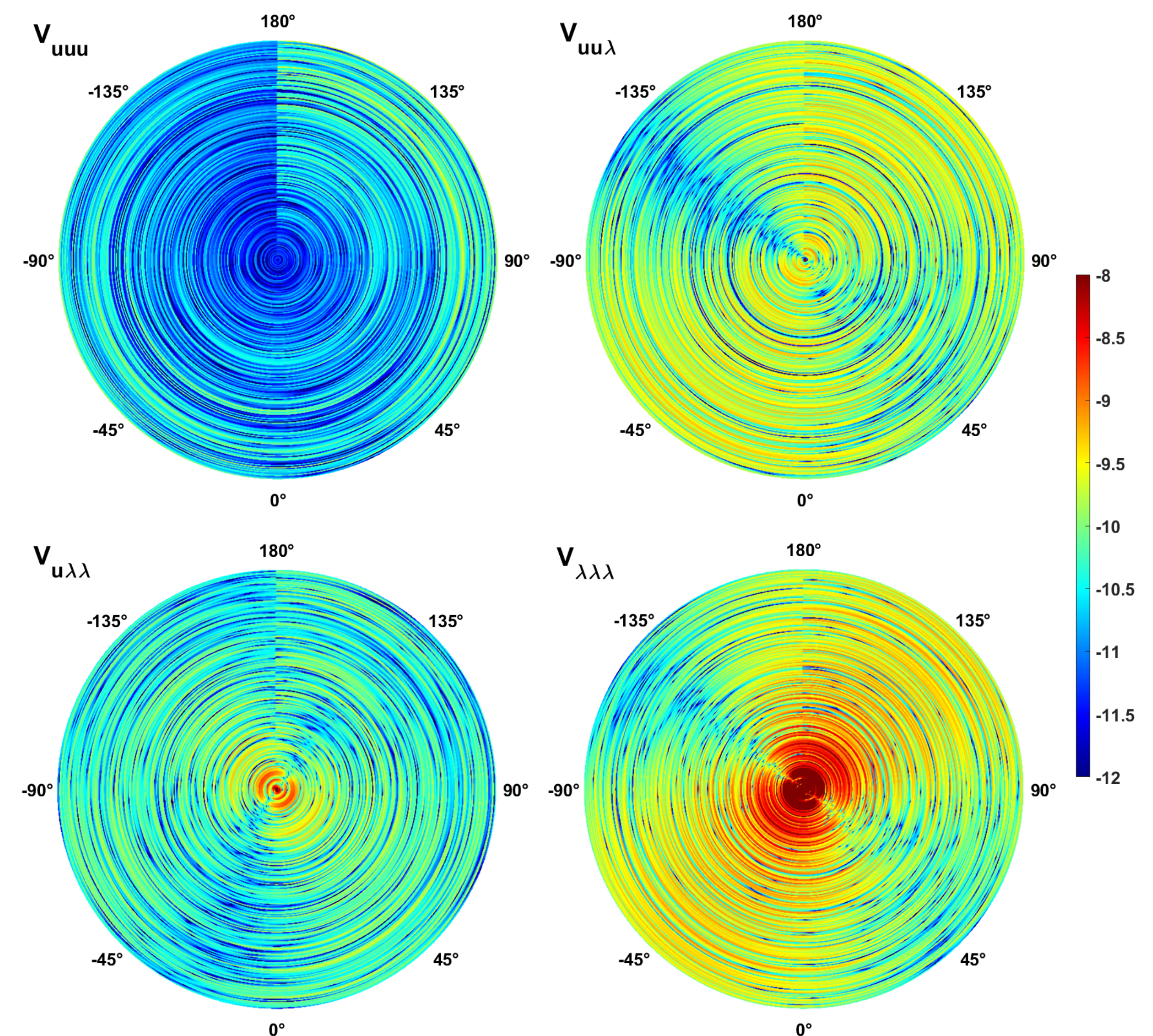


Fig. 2: Differences (\log_{10} of absolute differences) between the singular and the non-singular solution near the North Pole ($89.8^\circ \leq \beta \leq 90^\circ$) for selected derivatives.

To observe detailed discrepancies, we have examined differences along meridians (with 1° step between meridians) converging to the North Pole ($88^\circ \leq \beta < 90^\circ$). Example of above-mentioned discrepancies for the derivative $V_{\lambda\lambda\lambda}$ is depicted in Fig. 3. Similar behaviour was also observed for other derivatives with singularities in original expressions.

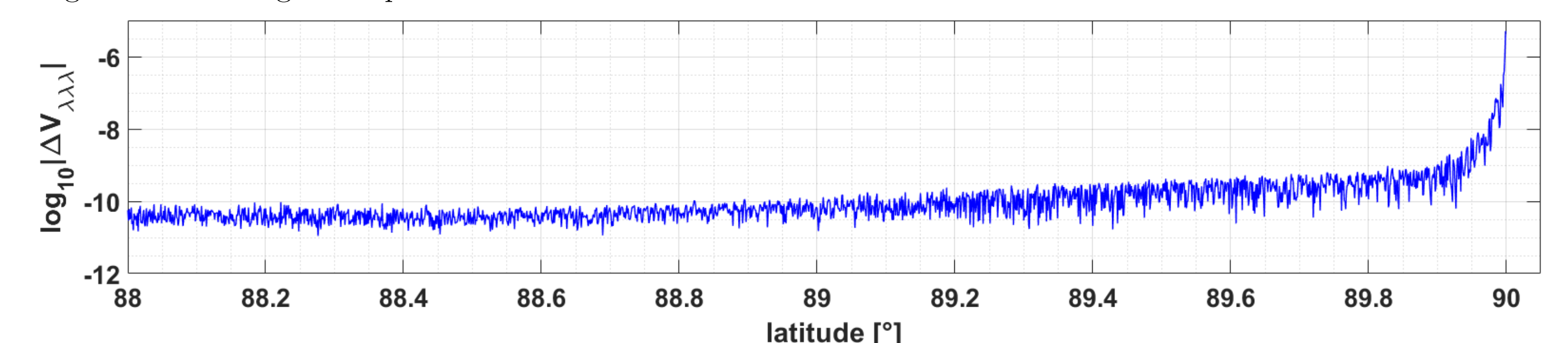


Fig. 3: Differences between the non-singular and the singular expressions for $V_{\lambda\lambda\lambda}$ close to the North Pole. y axis represents common logarithm of maximal error observed for given latitude.

Results of described experiment confirmed correctness of derived non-singular equations and their software implementation over non-polar regions, where the comparison with singular solution showed only negligible discrepancies. On the other hand, the increase of differences between singular and non-singular expressions over the polar regions complies with assumption about singular solution limitations.

Summary

- We have derived equations for the calculation of the gravitational potential and its derivatives up to the third order using the spheroidal harmonic functions method.
- We have conducted numerical experiment testing correctness of newly implemented non-singular expressions.
- Results indicate consistency of singular and non-singular solution over non-polar regions and increase of differences over polar regions.

Acknowledgements: Authors were supported by the project No. 23-07031S of the Czech Science Foundation.